# Resonant Goos-Hänchen and Imbert-Fedorov shifts at photonic crystal slabs

Thomas Paul,* Carsten Rockstuhl, Christoph Menzel, and Falk Lederer
*Institute of Condensed Matter Theory and Optics, Friedrich Schiller University Jena, Max-Wien-Platz 1, D-07743 Jena, Germany*
(Received 19 October 2007; published 5 May 2008)

We show that a longitudinal (Goos-Hänchen) and a transverse (Imbert-Fedorov) beam displacement can be observed upon total internal reflection at two-dimensional photonic crystal slabs. By inspecting only the dispersion relation of the photonic crystal we derive qualitative criteria for the direction of the beam shift. Furthermore, it will be shown that the beam shift can be strongly enhanced at particular angles of incidence where Fabry-Pérot resonances of the slab are excited. The Renard model, which predicts the strength of the shifts based on the Poynting vector in the totally reflecting medium, has been adapted to quantitatively analyze the beam shift.

DOI: 10.1103/PhysRevA.77.053802 PACS number(s): 42.25.Bs, 42.25.Gy, 42.70.Qs

## I. INTRODUCTION

If light is totally reflected at an interface separating two homogeneous media, a small displacement can be observed between the beam center of the reflected and the incident beam. The Goos-Hänchen shift (GHS) [1] is usually related to a beam displacement in a plane given by the surface normal and the wave vector of the incident light, whereas the Imbert-Fedorov shift (IFS) [2,3] is usually related to a transverse beam displacement relative to this plane. The modulus of both shifts depends strongly on the parameters of the system, such as, e.g., the state of polarization, the angle of incidence, or the wavelength. For most cases both shifts appear simultaneously; with the exception that due to symmetry requirements for a pure TE or TM polarized illumination beam an IFS cannot be observed [4]. The magnitude of the GHS at a single interface is usually of the order of a wavelength. The IFS is typically an order of magnitude smaller [5]. If the single interface is replaced by a thin dielectric film a significant enhancement of the GHS can potentially be achieved if leaky thin film modes supported in this layer are excited. This occurs, as expected, only for well defined system parameters [6,7].

For a quantitative evaluation of the beam shifts at single interfaces or at multilayered structures, two different models exist. The first one is usually referred to as the Artmann model [8]. It derives explicit expressions for the beam shifts in terms of the gradient of the reflected beam's phase in the reciprocal space. The second one is usually referred to as the Renard model [9]. It is based on considerations of the energy transport provided by evanescent waves in the totally reflecting medium parallel to the interface or by leaky thin film modes excited in the thin film, respectively. In the latter model the GHS and the IFS are given by

$$L_{\mathrm{GHS}} = \frac{1}{S_z^R}\int_0^\infty S_\parallel(z)dz, \tag{1}$$

$$L_{\mathrm{IFS}} = \frac{1}{S_z^R}\int_0^\infty S_\perp(z)dz. \tag{2}$$

$S_z^R$ denotes the $z$ component (defined here as normal to the surface) of the Poynting vector of the reflected beam at the interface $z=0$. $S_\parallel$ ($S_\perp$) denotes the Poynting vector component parallel (perpendicular) to the plane of incidence for $z \geq 0$. In case of reflection at a single interface the integration in Eqs. (1) and (2) will be performed over the evanescent field in the totally reflecting medium. For the homogeneous thin film setup the integration extends over the film and the adjacent region in which the transmitted field will decay evanescently (see Ref. [6]).

The pertinent setup of the present study is shown in Fig. 1. There, two homogeneous isotropic media having refractive indices $n_1$ and $n_3$ (with $n_1 > n_3$) are separated by a 2D photonic crystal (PC) slab. The surface normal is chosen to

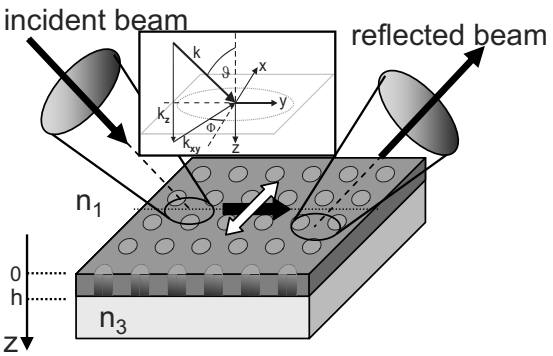


FIG. 1. General setup showing the reflection of a beam incident from a homogenous medium $n_1$ onto a 2D PC slab structure which is followed by the medium $n_3$. In the present example the values for the refractive indices are $n_1=3.5$ (silicon @1.5$\mu$m) and $n_3=1.0$ (air). The PC slab consists of a square lattice of air holes in the silicon having a radius of $r=0.3a$ (with $a$ being the lattice constant). The height of the slab is subject to modifications within our considerations. The arrows indicate the directions of the expected beam shifts relative to the plane of incidence. The thick black arrow represents the GHS and the thick white arrow represents the IFS. The inset shows the definition of an arbitrary wave vector $k$ in the underlying coordinate system that is attached to the PC structure.

*thomas.paul@uni-jena.de

 

be parallel to the $z$ direction. The structure is illuminated with a focused inclined beam which penetrates into the PC slab and which is totally reflected on the interface at $z=h$. The incident beam has a Gaussian shape in the plane of the interface at $z=0$. One comment has to be given concerning a potential realization of such a setup, as in all realistic experiments the light beam will incident generally from free space. Therefore, it has to be coupled appropriately to the incident medium. To achieve total internal reflection at the interface to the medium with refractive index $n_3$ one has to use, e.g., a devoted prism setup to couple light into the optical thicker medium $n_1$. This strategy is used for instance in Refs. [6] and [10]. Similar setups are also regularly used to excite surface plasmon polaritons, e.g., in the Otto or in the Kretschmann configuration. The ratio between the lattice period and the wavelength (inside the medium $n_1$) is slightly greater than 1/2 (about 0.6). Thus only the zeroth reflection order appears, except for large incidence angles near the edge of the first Brillouin zone. Recent work addressed similar problems [11,12]. There, the generalized Artmann model was applied for the calculation of the beam shifts. The longitudinal and transverse beam displacements have been calculated by evaluating the dependency of the reflection coefficient on the incident angle. The disadvantage of this approach is the evident lack of physical insight because the grating geometry and the reflection coefficients are cumbersome, if not to say impossible, to relate if the feature size of the structure is comparable to the wavelength. This holds for the present case.

By resorting to Renard's model [Eqs. (1) and (2)], a simpler association based on physical grounds of the expected GHS and IFS can be drawn by considering the Poynting vector of the field inside the PC slab. This assumes that the contribution of the evanescent field in medium $n_3$ to the shift is negligible as compared to the contribution of the PC slab.

Representing the incident beam only by its central plane wave component $\mathbf{k}_0$ the excited field inside the PC slab can be described by a superposition of forward and backward propagating Bloch modes with respect to the $z$ coordinate such that a standing wave establishes—in analogy to the superposition of plane waves in a homogeneous thin film. This consideration holds for a sufficiently small spectrum of the input beam, so that the variation of the optical response is negligible.

Therefore, by merely analyzing the Bloch modes and the dispersion relation of the underlying 2D PC it is possible to predict the direction of the beam displacement. This holds because the Poynting vector of a particular Bloch mode with a wave vector $\mathbf{k}_0$ is given by the normal derivative of the isofrequency surface $\mathbf{S} \propto \partial\omega / \partial \mathbf{k}_0$ at that point. The strength of the shift (or the modulus of the Poynting vector), however, depends on the coupling to the external field; but this information is inaccessible by using eigenmode calculations only. For the computation of the dispersion relation we used the well-established solver for the corresponding eigenvalue problem [13,14].

In this paper we shall analyze both the transverse and longitudinal beam shift upon reflection at a PC slab. Qualitative predictions of the beam shifts can be derived by using the Renard model and analyzing the Bloch modes of the two-dimensional PC. To prove the versatility of this approach, we outline at two examples how to identify domains in the dispersion relation where either a pure GHS or the combination of GHS and IFS occur simultaneously. Based on symmetry considerations it will be argued that a pure IFS cannot be observed for a two-dimensionally confined incident beam. To complete our study, we verify the quantitative validity of Renard's model for these examples. Results are compared with rigorous computations of the beam displacement in real space.

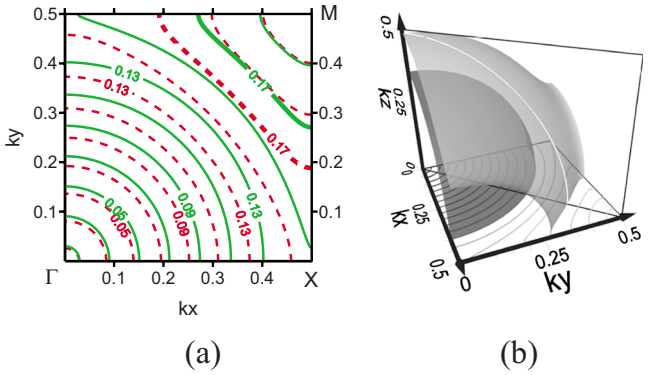


FIG. 2. (Color online) (a) Isofrequency curves of the first band of the infinite 2D photonic crystal for TE (red, dashed) and TM (green, solid) polarized light (shown is the first quadrant of the Brillouin zone). The wave vector component normal to the PC plane $k_z$ is kept zero. (b) Isofrequency surfaces (TM-like) for two different frequencies [$\omega=0.13$ (dark gray), $\omega=0.17$ (light gray)]. Here the dependence on the $k_z$ component is accounted for. The frequency values for negative $k_z$ are identical.

## II. GEOMETRY AND DISPERSION RELATION OF THE PERTINENT STRUCTURE

In the following the refractive index for the incident medium of the structure under investigation is assumed to be $n_1=3.5$. It corresponds in good approximation to the refractive index of silicon at a wavelength of 1.5 $\mu$m. The medium in the transmitted region is air ($n_3=1.0$). The PC slab is assumed to be made of air holes with a radius of $r=0.3a$ arranged in a square lattice with lattice constant $a$. The slab background medium is silicon with a refractive index of $n=n_1=3.5$. The height of the slab and the operational frequency are subject to variations in the analysis.

Figure 2(a) shows the isofrequency curves of the infinitely extended PC for the first band of the two independent polarizations TM (electric field in the $z$ direction) and TE (magnetic field in the $z$ direction). The TE (TM) band covers a frequency range from $\omega=0\ldots0.2194$ ($0\ldots0.2045$), where the normalized frequency is given in units of $2\pi c/a$. The second TE (TM) band commences at $\omega=0.2153$ (0.1791), indicating a small overlap with the first band. However, this is of no importance because all studies are undertaken for lower frequencies. By calculating the entire 3D dispersion relation $\omega=\omega(k_x,k_y,k_z)$ the strict separation in TE and TM polarization is no longer valid and the first two lowest bands strongly overlap. Nonetheless, in case of an incident field

along high symmetry directions these two polarization states can be excited independently. By choosing an adequate polarization for the incident field it is possible to excite Bloch modes of a single photonic band only, so that cross-coupling effects can be avoided. We will take advantage of this fact later in looking at the pure GHS where light is incident along the $\overline{\Gamma M}$ direction. In what follows bands of the 3D dispersion relation converging for $k_z=0$ toward the original TM (TE) polarization states will be called "TM(TE)-like."

Figure 2(b) shows two isofrequency surfaces (TM-like only) for the frequencies $\omega=0.13$ and $\omega=0.17$. The isofrequency surface at $\omega=0.13$ exhibits an almost spherical shape comparable to that of a homogeneous medium. However, if an isofrequency surface (for instance, at $\omega=0.17$) approaches the boundary of the Brillouin zone at $k_{x/y}=\pm 0.5\ 2\pi/a$ the sphere experiences deformations and the edges become deformed. The derivative of the frequency with respect to at least one wave vector component always vanishes. This is an effect of the inversion symmetry $(x \leftrightarrow y)$ of the pertinent photonic crystal which leaves $\partial\omega/\partial k_x|_{0.5} = \partial\omega/\partial k_x|_{-0.5} = \partial\omega/\partial k_y|_{0.5} = \partial\omega/\partial k_y|_{-0.5} = 0$ to be the only solution. Throughout the remaining article all wave vector quantities are dimensionless due to the normalization in units of $2\pi/a$.

To estimate the beam shift upon reflection at the PC slab, the coupling of the illuminating field to the eigenmodes of the PC has to be considered. Under illumination by a plane wave or a paraxial beam (that is a beam which is a solution to the paraxial wave equation) being characterized by a principal wave vector $\mathbf{k}^{(1)}=(k_x^{(1)},k_y^{(1)},k_z^{(1)})$ coupling requires continuity of the transverse components of the wave vectors at the interface. Coupling can also be accomplished by adding an integer multiple of the reciprocal lattice vector to the wave vector component of the incident beam, as

$$(k_x^{(2)},k_y^{(2)}) = (k_x^{(1)},k_y^{(1)}) + (m_x R_x, m_y R_y), \tag{3}$$

where $\mathbf{k}^{(2)}=(k_x^{(2)},k_y^{(2)},\pm k_z^{(2)})$ denotes the Bloch vector of the potentially excited modes [see also Fig. 2(b)] in the PC slab. By restricting the operational frequencies to values less than $\omega=0.1791$ where only the first two bands (TM-like and TE-like) are accessible, coupling takes place to only one pair of forward and backward propagating Bloch modes in each polarization.

## III. THE GOOS-HÄNCHEN SHIFT

In this section a setup is analyzed that allows for the observation of a pure GH shift. As mentioned above, only frequencies smaller than $\omega=0.1791$ are considered. By inspecting the isofrequency curves (Fig. 2) it can be seen that

$$\vec{\nabla}_{k_x,k_y}\omega(k_x,k_y,k_z)|_{\overline{\Gamma M}} \propto \overline{\Gamma M}. \tag{4}$$

This directly implies that the transverse component of the Poynting vector $(S_x,S_y)$ is parallel to the transverse wave vector component for all modes in $\overline{\Gamma M}$ direction where the high symmetry points $\Gamma$ and $M$ themselves must be excluded because the group velocity and hence the derivative will vanish. Again, Eq. (4) is a consequence of the inversion symmetry of the chosen structure along the $x$-$y$ axis, which corresponds to the $\Gamma M$ direction in reciprocal space. Therefore, an IFS is not observable. No energy is transported normal to the plane given by the incident vector and surface normal. Moreover, by varying the incident angle and keeping all other parameters (such as the frequency and the slab thickness) fixed Fabry-Pérot (FP) resonances will occur. The strength of the expected beam shift will be influenced by such resonances due to the field enhancement inside the slab.

To prove these predictions we applied the following computational strategy: First, the transmission coefficients of a single plane wave as a function of the angle of incidence were investigated in order to identify FP resonances. Secondly, a finite input beam (simulated by a superposition of a set of plane waves) was used to calculate the reflected field distribution at the interface $z=0$. From these simulations the beam shift can be exactly evaluated by calculating the center of gravity of the amplitude profile of the reflected beam. Subsequently, the principle angle of incidence is varied to determine the beam displacement as a function of this angle. In all situations analyzed herein the scattering problem of a single plane wave at a PC slab has to be solved rigorously. This is done by using the Fourier modal method (FMM) [15,16]. It is a rigorous diffraction theory that makes use of a Fourier decomposition of all quantities in the biperiodic system, namely, the electric and the magnetic field components and the dielectric structure. A sufficiently large number of Fourier orders (here, $21\times 21$) was retained in the simulation to ensure convergence of all derived quantities. Alternatively to the evaluation of the reflected beam's center of gravity, Renard's model is employed for a quantitative analysis of the beam shifts using Eqs. (1) and (2). The Poynting vector of the field inside the PC slab is provided again by FMM calculations. Comparing these results allows us to assess the accuracy of Renard's model applied to the case of a PC slab.

To get started the dependence of the transmitted amplitude on the incident angle and the polarization is investigated. The illuminating plane wave is characterized by a wave vector

$$\mathbf{k}_0^{(1)} = \frac{2\pi}{\lambda_0} n_1[\sin\vartheta\cos\phi, \sin\vartheta\sin\phi, \cos\vartheta]. \tag{5}$$

For the $\Gamma M$ direction $\phi=45°$ (see the inset of Fig. 1). The frequency is chosen to be $\omega=0.17$. By fixing the PC period to $a=0.255\ \mu$m the frequency corresponds to a free space wavelength of $\lambda_0=1.5\ \mu$m. Furthermore the thickness of the slab is $h=5.5a=1.4\ \mu$m. This value constitutes a compromise between, on the one hand, well-pronounced FP resonances and, on the other hand, manufacturing feasibility.

The calculations have been performed for the two independent polarizations $\mathrm{TE}^{\mathrm{inc}}$ $(\mathbf{E}\perp\mathbf{k}_0\perp\hat{\mathbf{z}})$ and $\mathrm{TM}^{\mathrm{inc}}$ $(\mathbf{H}\perp\mathbf{k}_0\perp\hat{\mathbf{z}})$. The superscript "inc" refers to the polarization states inside the substrate. Comparing them to the TE-like and TM-like polarization states of the photonic crystal they have the same dominant field components in each case.

Figure 3(a) shows the calculated modulus of the zeroth order amplitude transmission coefficient $T_{00}=\sqrt{|T_{00,x}|^2+|T_{00,y}|^2+|T_{00,z}|^2}$ depending on the polarization at the exit surface of the PC slab at $z=h$. In the parameter range

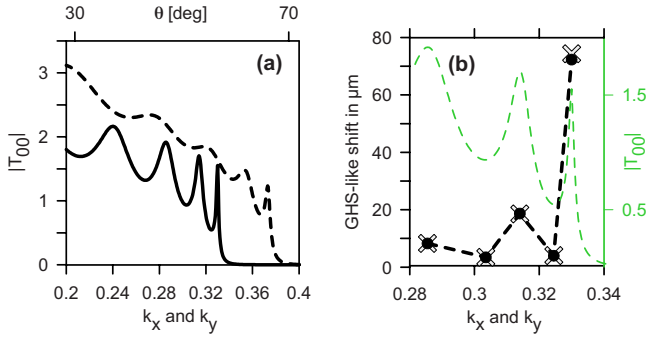


FIG. 3. (Color online) (a) Modulus of the zeroth order amplitude transmission coefficient $|T_{00}|$ as a function of the transverse wave vector. The wave vector is oriented along the $\overline{\Gamma M}$ direction. The solid line represents the values for $TE^{inc}$ polarization and the dashed line for $TM^{inc}$ polarization. (b) GHS as a function of the angle of incidence at illumination along the $\overline{\Gamma M}$ direction in $TE^{inc}$ polarization. The thick black circles show the GHS calculated by analyzing the center of gravity of the propagating reflected beam. The crosses indicate results obtained by employing the generalized Renard model. The green dashed line shows the modulus of the amplitude transmission coefficient $|T_{00}|$ and illustrates the angular positions of the FP resonances inside the PC slab.

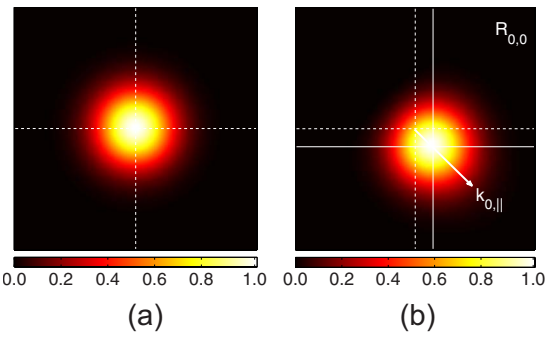


FIG. 4. (Color online) (a) Amplitude profile of the incident and (b) the propagating reflected beam at the interface $z=0$. The principal beam direction is characterized by $\phi=45°$ ($\Gamma M$) and $\theta=51.66°$. It is indicated by the white arrow in (b). This allows for the excitation of the lowest order FP resonance in the PC slab. The width of the depicted section in both transverse dimensions is $2500a=637.5$ $\mu$m.

depicted for the incident angle (or $k_x$ and $k_y$, respectively) the light is always totally reflected at the interface between the PC slab and the air region. This causes all transmitted orders to be evanescent, including the zeroth one. Consequently, there is no energy transfer into the air but the peaks of the amplitude transmission coefficient allow to probe the presence of Fabry-Pérot resonances. Two clearly distinguishable cutoff values exist for the amplitude transmission coefficient at $k_{x,y}^{TE\ cut}\simeq 0.335$ and $k_{x,y}^{TM\ cut}\simeq 0.38$. This is a hint that there is no cross coupling between the two incident polarizations. For larger values of the wave vector total internal reflection appears already at the interface between silicon and the PC slab. In fact, by calculating the overlap integral between the incident plane wave and the corresponding Bloch modes, it turns out that for incident $TE^{inc}$ polarization a coupling occurs only to the TE-like Bloch modes and vice versa. No cross coupling among the polarizations could be identified. Furthermore it can be seen that the transmission contrast (it will be understood here as the ratio of the peak value to the nearest minimum value) of the resonances for $TE^{inc}$ polarization is much larger compared to $TM^{inc}$. Hence it can be anticipated that in the TE case the beam shift is much more sensitive to variations in the angle of incidence, so that the following calculations are exclusively performed for $TE^{inc}$ illumination.

For the investigation of the beam displacement a paraxial finite input beam, constructed by a superposition of plane waves, is used. In the following example we consider an angular distribution with a Gaussian shape proportional to $\exp\{-[(k_x-k_{0,x})^2+(k_y-k_{0,y})^2]/\sigma_k^2\}$, with $\sigma_k=0.8\times10^{-3}$ $2\pi/a$. All plane waves of the spectrum are $TE^{inc}$ polarized. The vector $\mathbf{k_0}$ denotes the principle beam direction. Detailed information on the definition of the input beam by its spectrum of plane waves is given in the Appendix. The chosen spectral parameters correspond to an oblique incident, almost linear polarized beam with a Gaussian amplitude profile along the interface characterized by $\exp[-(x^2+y^2)/\sigma^2]$. The waist diameter is $2\sigma=(2)2/\sigma_k\simeq 800a$. The amplitude distribution of the incident beam straight at the surface of the PC slab ($z=0$) is shown in Fig. 4(a). It has to be mentioned that the concrete choice of the incident beam will not influence the principle observations. The only reason for its choice was to match its angular width with that of the FP resonances. It permits one to avoid amplitude distortions in the reflected field due to the sharp FP resonances.

In the relevant range of parameters it can be noticed that only the zeroth order reflected wave is propagating. All higher reflected orders are evanescent due to the small PC period. For an incident angle of $\vartheta=51.66°$ ($k_x=k_y=0.33$) the propagating reflected field at the interface $z=0$ is shown in Fig. 4(b). This incident angle corresponds to the angle for which the sharpest FP resonance in TE-like polarization is excited.

From the figure a displacement of the center of the reflected beam (indicated by the intersection of the solid white lines) as compared to the incident beam (dashed white lines) can be clearly seen. In this particular example the displacement of the beam is $L_x=L_y=200.5a=51.1$ $\mu$m. The overall pure GHS amounts therefore to $L_{GHS}=72.3$ $\mu$m. The center of the beam was determined by calculating the center of gravity of the beam's amplitude distribution $g(x,y)=\sqrt{|E_x(x,y)|^2+|E_y(x,y)|^2+|E_z(x,y)|^2}$, with vector $\mathbf{E}$ corresponding to the electrical field of the particular beam under consideration. The center of gravity is given by $L_x=\int xg(x,y)dxdy/\int g(x,y)dxdy$ and analogous for $L_y$. Although not visible from the figure but deducible by analyzing higher order momenta, it is noticed that the beam profile is slightly distorted as compared to the incident Gaussian profile. This can be attributed to the fact that the width of the resonance in the reciprocal space $\Delta_{FWHM}\approx 2\times10^{-3}$ $2\pi/a$ gets comparable to the width of the incident beam given by $2\sigma_k=1.6\times10^{-3}$ $2\pi/a$. The change in the magnitude of the reflection coefficient across the spectra causes such distortions. Furthermore the GHS was calculated at the maxima and minima of the amplitude transmission spectra, as shown

in Fig. 3(a). The maxima correspond to higher order FP resonances. The results are shown in Fig. 3(b) by the black circles. No IFS is observed for all analyzed cases as expected.

Additionally we calculated the beam shift using a generalized Renard-type model [see Eqs. (1) and (2)]. These results are shown in Fig. 3(b) as gray crosses. For this purpose the spatial average of the Poynting vector over a single unit cell was used for evaluating the appropriate integrals. The Poynting vector was numerically calculated by using the electromagnetic fields computed with the FMM. Only the zeroth reflected order was taken into account in calculating the normal component $S_z^R$ of the Poynting vector used in Eqs. (1) and (2), respectively. It can be noticed that both methods are in excellent agreement. The observed GHS increases dramatically at FP resonances. Accordingly, the strongest GHS is observed if the first FP resonance is employed. It amounts to $L_{\mathrm{GHS}}=72.3$ $\mu$m as already mentioned. The GHS in the adjacent minimum is only as small as $L_{\mathrm{GHS}}=2.8$ $\mu$m.

## IV. THE COMBINED IMBERT-FEDOROV AND GOOS-HÄNCHEN SHIFT

Now we consider an example that allows the simultaneous observation of the GHS and the IFS. To this end we illuminate the PC film along the $XM$ direction which means that the transverse wave vector is restricted to $k_x=0.5$ and $0<k_y<0.5$. As the square lattice PC slab is obviously symmetric against inversion in the $x$ direction it can be concluded that the $k_x$ derivative of the dispersion relation vanishes at the Brillouin zone boundaries $k_x=\pm 0.5$. Therefore the transverse gradient writes as

$$\nabla_{k_x,k_y}\omega(k_x,k_y,k_z)|_{\overline{XM}}=(0,\partial\omega/\partial k_y)^T \tag{6}$$

provided that the separate bands do not degenerate. This is indeed true in the frequency range of interest. Analogous considerations can be performed for the $k_y=\pm 0.5$ boundary of the Brillouin zone. In the limit of $(k_x,k_y)=(\pm 0.5,0)=X$ the derivative in Eq. (6) must approach to zero because the group velocity vanishes at that point. Consequently, a pure IFS cannot be observed. Moreover, there will be no beam displacement observable at all at $(k_x,k_y)=X$ because the isofrequency surfaces take extreme values at that point. We verified this thesis by rigorous calculations (keeping $k_{x/y}$ fixed and varying $\omega$) but the results are not explicitly shown here. For further considerations we again analyze the beam shifts at a frequency of $\omega=0.17$. The geometry of the PC remained unaltered but the slab thickness was taken to be $h=13.5a$. The only purpose in doing so was to obtain sharper FP resonances for varying angle of incidence. All qualitative considerations hold for thinner films too.

As the structure is now operated at the boundary of the Brillouin zone two propagating reflected orders ($R_{00}$ and $R_{-10}$) exist. This may lead to some complications in the calculation of the beam displacement as will be shown later. Figure 5(a) shows the amplitude for the zeroth transmitted order $T_{00}$ at $z=0$ as a function of the angle of incidence. Evidently, the corresponding wave is evanescent.

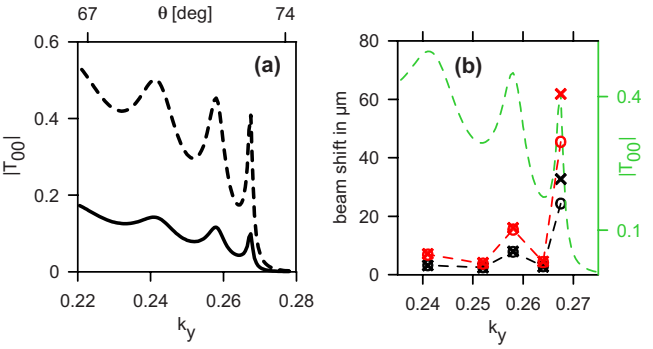


FIG. 5. (Color online) (a) Modulus of the zeroth order transmitted amplitude $|T_{00}|$ as a function of the incidence angle. The direction of incidence in the transverse direction is $\overline{XM}$. The solid and dashed lines indicate $\mathrm{TE}^{\mathrm{inc}}$ and $\mathrm{TM}^{\mathrm{inc}}$ polarization, respectively. $k_x$ has a fixed value of 0.5. (b) The black circles show the GHS upon analyzing the profile of the propagating reflected beam (zeroth $R_{00}$ and minus first order $R_{-10}$) and determining the displacement of the center of gravity relative to the incident beam. The red circles show the IFS. Crosses with the same color indicate the same quantities but determined using the generalized Renard model. The underlying green dashed curve shows the transmission spectrum $|T_{00}|$ and illustrates the location of the FP resonances in the PC slab. The polarization is $\mathrm{TM}^{\mathrm{inc}}$.

In contrast to the previous case the cutoff values $k_y^{\mathrm{TE\ cut}}$ and $k_y^{\mathrm{TM\ cut}}$ for transmission are identical in the present configuration amounting to $k_y\approx 0.27$. For larger values the field is already totally internal reflected at the interface between the silicon cladding and the PC slab.

The determined cutoff value coincides with the band edge of the TM-like Bloch modes in the $XM$ direction of the 2D PC. This can be seen from Fig. 2(a).

Furthermore the band edge for TE-like polarization is located at $k_y=0.19$. Consequently, only TM-like modes can be excited in that parameter range as shown in Fig. 5(a), so that a cross coupling between $\mathrm{TE}^{\mathrm{inc}}$ and TM-like polarized Bloch waves takes place. Only one pair of forward and backward propagating Bloch modes is excited inside the PC slab simultaneously, similar to the previously discussed case in Sec. III.

By calculating the reflection of the same illuminating Gaussian beam as in Sec. III, but now with $\mathrm{TM}^{\mathrm{inc}}$ polarization (it was chosen because the FP resonances are more pronounced), a remarkable beam displacement, exclusively in the $y$ direction, is observed. The values for the beam shift in the $x$ direction fluctuate around zero within a range of one lattice constant. This is attributed to a finite numerical precision and is of no importance to the present study. Figure 5(b) shows results of the beam displacement converted into its Goos-Hänchen (parallel to the transverse wave vector) and Imbert-Fedorov (perpendicular to the transverse wave vector) portions. The calculation of the shift was done first by analyzing the center of gravity of the reflected field as compared to the incident field and second by employing the generalized Renard model as was done before.

For the specific input conditions chosen the simultaneous appearance of IFS and GHS is observed. The IFS is, contrary to what is usually observed, even stronger than the GHS. The IFS takes a maximum value of 45 $\mu$m in the first FP reso-

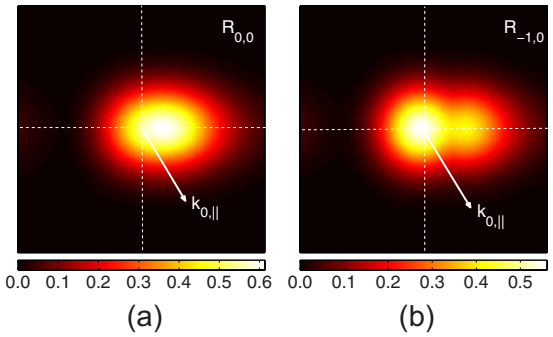


FIG. 6. (Color online) Amplitude profile of the (a) zeroth order and the (b) minus first order reflected beam on the interface $z=0$. The main beam direction characterized by $k_x=0.5$ and $k_y=0.2675$ (first FP resonance) is indicated by the white arrows. The width of the depicted section is $2500a=637.5$ $\mu$m.

nance. Compared to other values known from homogeneous media interfaces [5,6] we designate the present value as a giant IFS. Furthermore it can be seen that a certain difference exists concerning the predicted strength of the beam displacement employing the two different methods. The difference is strongest for the beam displacement at an angle of incidence corresponding to the first FP resonance. The differences amount to $\Delta_{\mathrm{IFS}}=17$ $\mu$m and $\Delta_{\mathrm{GHS}}=9$ $\mu$m.

We attribute this discrepancy to the appearance of two propagating orders in reflection. An implicit assumption of Renard's model according to Eqs. (1) and (2) is that the two propagating orders will experience the same amount of beam displacement. For this particular case the beam displacement can be separately shown for both propagating reflection orders. Figure 6 shows the displacement for an angle of incidence corresponding to the first FP resonance. The white lines indicate the coordinate axis.

From the figure it can be clearly seen that the two propagating orders experience different beam displacements. Furthermore both beams are distorted. The distortion is more pronounced for the minus first diffraction order. In this case the effective displacement of the center of gravity is primarily caused by the distortion of the beam rather than by the shift of the maximum of the amplitude profile.

Moreover, by using Renard's model we have neglected all possible vectorial effects in the sense that each field component may experience a different shift. Indeed, by evaluating the displacement of the beam for each vectorial component separately strong differences are observable. Nevertheless, these effects do not chance the principal observations, that, at least qualitatively, the expected beam shift can be predicted by the generalized Renard model that employs the vectorial Poynting vector field.

## V. CONCLUSION

In this article we identified the peculiarities of beam displacements occurring upon total internal reflection on a photonic crystal slab. This is accomplished by generalizing the classical Renard model. Basically the generalization allows to link the expected shift of the beam to the dispersion relation of the underlying 2D PC. Based on symmetry considerations it could be exemplified that there are configurations where either a pure GHS or the combination of a GHS and an IFS occurs. In addition, Fabry-Pérot resonances of the PC slab were exploited to dramatically enhance the beam displacements, leading to the observation of a giant GHS and IFS. GHSs and IFSs over 48λ (72 $\mu$m) and 30λ (45 $\mu$m) were observed using a PC slab with a thickness of only 1.4 $\mu$m and about 3.45 $\mu$m in the respective examples. The strength of the GHS compares well with values known from literature for homogeneous dielectric slabs with a magnitude of about 50λ [6]. More important, the IFS largely exceeds previously reported values, which did not exceed one wavelength for homogeneous media interfaces [5,6].

For the future it is expected, that also a negative GHS is observable on 2D-photonic crystal slab interfaces. Within the presented model this implies the need to find propagation directions in which the angle between the wave vector and the Poynting vector exceeds 90°. This can be achieved, for example, for incident angles which are located within a higher Brillouin zone or by working within higher order bands which exhibit negative refraction. In general it is expected that the beam displacement in special directions can be forecasted using general symmetry properties of the underlying crystal and therewith of the associated dispersion relation.

On the other side the model has certain limitations if the reflected field is composed of more than a single diffraction order as argued in the previous section. Strictly speaking, this will restrict the applicability of the method to PCs with a period sufficiently small as compared to the wavelength. Nevertheless, we believe that at least the principal beam shift direction (according to the measured center of gravity) goes along with the presented model.

## APPENDIX: COMPUTATIONAL DETAILS

To provide a concise picture of the applied computational procedure, we will give in the following section a detailed outline of the employed approach. Emphasis is put on the definition of the incident wave field. A time dependency of $\exp(-i\omega t)$ for any electromagnetic field is assumed. For the rigorous solution of the scattering problem of a beam incident on a photonic crystal slab, the Fourier modal method (FMM) was used [15,16]. The FMM provides the rigorous solution for the scattering of a plane wave of arbitrary angle of incidence and polarization at an arbitrary biperiodic structure. To apply this method to a finite sized monochromatic illuminating wave field, this beam has to be decomposed into an angular spectrum of plane waves. The functional dependence of the angular spectrum

$$\mathbf{E}(\mathbf{k}) = \int_{-\infty}^{\infty} d^3\mathbf{r}\mathbf{E}(\mathbf{r})\exp[-i\mathbf{k}\cdot\mathbf{r}] \tag{A1}$$

is simply given by a Fourier transformation of the field distribution in the real space. On the other hand, every superposition of an arbitrary set of plane waves $\mathbf{E}(\mathbf{k})$ will lead to a spatial field distribution $\mathbf{E}(\mathbf{r})$ [applying the inverse trans-

formation of Eq. (A1)] that rigorously obeys Maxwell's equations. In the present manuscript the incident beam is constructed out of an angular spectrum of plane waves with a Gaussian amplitude distribution in $k$ space centered around the principle beam direction $\mathbf{k_0}$. Furthermore, all plane waves of the spectrum have the same polarization, either TE or TM. Therefore, the angular distribution can be written as

$$\mathbf{E}(\mathbf{k}) = \mathbf{e}(\mathbf{k}) E_0 \exp\left\{ - \frac{(k_x - k_{0,x})^2 + (k_y - k_{0,y})^2}{\sigma_k^2} \right\}. \quad \text{(A2)}$$

Hereby, $\mathbf{e}(\mathbf{k})$ is the electrical field vector of a single plane wave with wave vector $\mathbf{k}$, which is normalized to unity. $\sigma_k$ is a measure for the spectral width of the beam and $E_0$ represents the maximal amplitude value. Assuming that the wave vector $\mathbf{k} = 2\pi n/\lambda_0 (\sin\theta\cos\phi, \sin\theta\sin\phi, \cos\theta)^T$ is given in spherical coordinates with the azimuthal and the polar angle being $\phi$ and $\theta$, the normalized electrical field vector of the associated plane wave is given by

$$\mathbf{e}(\mathbf{k}) = \mathbf{e}(\phi, \theta, \xi) = \begin{pmatrix} \cos\xi\cos\theta\cos\phi - \sin\xi\sin\phi \\ \cos\xi\cos\theta\sin\phi + \sin\xi\cos\phi \\ -\cos\xi\sin\theta \end{pmatrix}. \quad \text{(A3)}$$

$\xi$ is the polarization angle which can take values in the interval $[0, 2\pi]$. In all calculations performed in this work the polarization was chosen to be only pure TE ($\xi = \pi/2$) or pure TM ($\xi = 0$), respectively. For a sufficiently small width $\sigma_k$ of the spectrum the associated beam in the spatial domain has a Gaussian distribution with a dominating field vector either in TE or TM polarization. Nevertheless, by virtue of this rigorous description there are also field components which cause a distortion of the beam from the purely linear polarized Gaussian state. Their strength tends to zero the smaller the spectral width gets. In the present work the spectral width was chosen to be sufficiently small such that the amplitude distribution of the complete incident beam on the interface is perfectly Gaussian with no measurable deviations. More information about the peculiarities on the representation of a finite input beam by its spectrum of plane waves is given, e.g., in Ref. [4].

Equations (A1) and (A2) are also valid for the associated magnetic field, provided that $\mathbf{E}$ and $\mathbf{e}$ are replaced by the magnetic quantities $\mathbf{H}$ and $\mathbf{h}$. The linkage between the field components $\mathbf{e}(\mathbf{k})$, $E_0$ and $\mathbf{h}(\mathbf{k})$, $H_0$ is directly given by Maxwell's curl equation $\nabla \times \mathbf{E} i\omega\mu_0 \mathbf{H}$ which gives

$$\mathbf{h}(\mathbf{k}) = \mathbf{h}(\phi, \theta, \xi) = \begin{pmatrix} -\sin\xi\cos\theta\cos\phi - \cos\xi\sin\phi \\ -\sin\xi\cos\theta\sin\phi + \cos\xi\cos\phi \\ \sin\xi\sin\theta \end{pmatrix},$$

$$H_0 = \sqrt{\frac{\epsilon_0}{\mu_0}} n E_0. \quad \text{(A4)}$$


[1] F. Goos and H. Hänchen, Ann. Phys. **436**, 333 (1947).
[2] F. I. Fedorov, Dokl. Akad. Nauk SSSR **105**, 465 (1955).
[3] C. Imbert, Nouv. Rev. Opt. Appl. **3**, 199 (1972).
[4] C. Menzel, C. Rockstuhl, T. Paul, S. Fahr, and F. Lederer, Phys. Rev. A **77**, 013810 (2008).
[5] C. Imbert, Phys. Rev. D **5**, 787 (1972).
[6] F. Pillon *et al.*, J. Opt. Soc. Am. B **22**, 1290 (2005).
[7] I. V. Shadrivov, A. A. Zharov, and Y. S. Kivshar, Appl. Phys. Lett. **83**, 2713 (2003).
[8] K. Artmann, Ann. Phys. **437**, 87 (1948).
[9] R. H. Renard, J. Opt. Soc. Am. **54**, 1190 (1964).
[10] H. Gilles, S. Girard, and J. Hamel, Opt. Lett. **27**, 1421 (2002).
[11] R. Güther, B. H. Kleemann, J. Elschner, and G. Schmidt, J. Mod. Opt. **49**, 1785 (2002).
[12] F. Falco, T. Tamir, and K. M. Leung, J. Opt. Soc. Am. A **24**, 1666 (2007).
[13] S. G. Johnson and J. D. Joannopoulos, Opt. Express **8**, 173 (2001).
[14] S. G. Johnson and J. D. Joannopoulos, http://ab-initio.mit.edu/wiki/index.php/MIT_Photonic_Bands
[15] E. Noponen and J. Turunen, J. Opt. Soc. Am. A **11**, 2494 (1994).
[16] L. Li, J. Opt. Soc. Am. A **13**, 1870 (1996).